Nucleation of transition waves via collisions of elastic vector solitons

H. Yasuda,[1,2] H. Shu,[1] W. Jiao,[1] V. Tournat,[3] and J. R. Raney*[1]

[1]*Department of Mechanical Engineering and Applied Mechanics, University of Pennsylvania, Philadelphia, Pennsylvania 19104, USA*
[2]*Aviation Technology Directorate, Japan Aerospace Exploration Agency, Mitaka, Tokyo 1810015, Japan*
[3]*Laboratoire d'Acoustique de l'Université du Mans (LAUM), UMR 6613, Institut d'Acoustique - Graduate School (IA-GS), CNRS, Le Mans Université, Le Mans, France*

In this work, we show that collisions of one type of nonlinear wave can lead to generation of a different kind of nonlinear wave. Specifically, we demonstrate the formation of topological solitons (or transition waves) via collisions of elastic vector solitons, another type of nonlinear wave, in a multistable mechanical system with coupling between translational and rotational degrees of freedom. We experimentally observe the nucleation of a phase transformation arising from colliding waves, and we numerically investigate head-on and overtaking collisions of solitary waves with vectorial properties (i.e., elastic vector solitons). Unlike KdV-type solitons, which maintain their shape despite collisions, our system shows that collisions of two vector solitons can cause nucleation of a new phase via annihilation of the vector solitons, triggering the propagation of transition waves. The propagation of these depends both on the amount of energy carried by the vector solitons and on their respective rotational directions. The observation of the initiation of transition waves with collisions of vector solitons in multistable mechanical systems is an unexplored area of fundamental nonlinear wave interactions, and could also prove useful in applications involving reconfigurable structures.

PACS numbers:

Nonlinear wave phenomena have long been of significant interest among researchers, both as an object of fundamental curiosity and for their potential in a variety of applications. Solitons, in particular, have long been studied in contexts ranging from the Fermi-Pasta-Ulam-Tsingou lattice and KdV equation [1–3] to granular media [4–7], soft matter (e.g., liquid crystals) [8, 9], etc. Generally, solitons are characterized as localized wave packets propagating with a constant speed and shape in the presence of nonlinearity and dispersion. Moreover, solitons keep their shape even if they collide with other solitons, analogous to the behavior of particles.

More recently, flexible mechanical metamaterials have been designed that derive their nonlinearity from large internal rotations [10], enabling previously unexplored nonlinear wave phenomena. For example, unlike solitons in classical 1D systems (e.g., granular crystals [4, 7]), a system of rotating squares, in which each element has translational and rotational degrees of freedom (DOF), can exhibit the propagation of vector solitons with coupling between these DOFs [10–12] (i.e., vectorial nature), cnoidal waves [13], and "sound bullets" [14]. The coupling of multiple DOFs also enables rich collision behavior, including collisions analogous to classical soliton collisions, but also repelling, destruction, etc. [15].

Moreover, multistable versions of these systems can support propagation of transition waves (or topological solitons), an effect that may be introduced via geometric constraints, permanent magnets, etc. [16–24]. Transition waves are propagating nonlinear wave fronts that sequentially switch the structural elements from one stable state to another [10, 16]. Recent research efforts on the observation, manipulation, and applications of transition waves in mechanical systems [22, 25] provide a macroscopic analogy with the fundamental processes of dynamic phase transitions [26, 27], phase transformations in crystalline materials [28, 29], and damage propagation in solids [30, 31].

In this work, we demonstrate that colliding vector solitons can annihilate to nucleate a phase transition in multistable mechanical systems (i.e., the vector solitons cease to exist when the new phase is nucleated). The new phase can subsequently propagate outward in the form of a transition wave. While transition waves have been previously triggered at the edge of multistable mechanical metamaterials [16, 18, 32, 33], we demonstrate here that soliton collisions can effectively initiate transition waves at arbitrary locations in the structure (governed by the timing and amplitude of impulses at the ends of the structure). Our findings provide insight about the fundamental interactions between different types of nonlinear waves, and may in the future be relevant to engineering applications related to deployable structures, reconfigurable robots, etc.

We start by experimentally exploring wave interactions in a multistable system by employing a 1D chain prototype composed of rotating squares and hinges (Fig. 1(a)). Since, in the experiments, damping and friction hinder the propagation of energy carried from the initial pulses, we have adjusted the energy landscape through a pre-rotation of 15° to reduce the energy required to induce nucleation of the new phase (Fig. 1(b)) [17]. We define u_n and θ_n as the relative displacement and rotational angle of the squares in the nth column (corresponding to the

*Corresponding author, raney@seas.upenn.edu

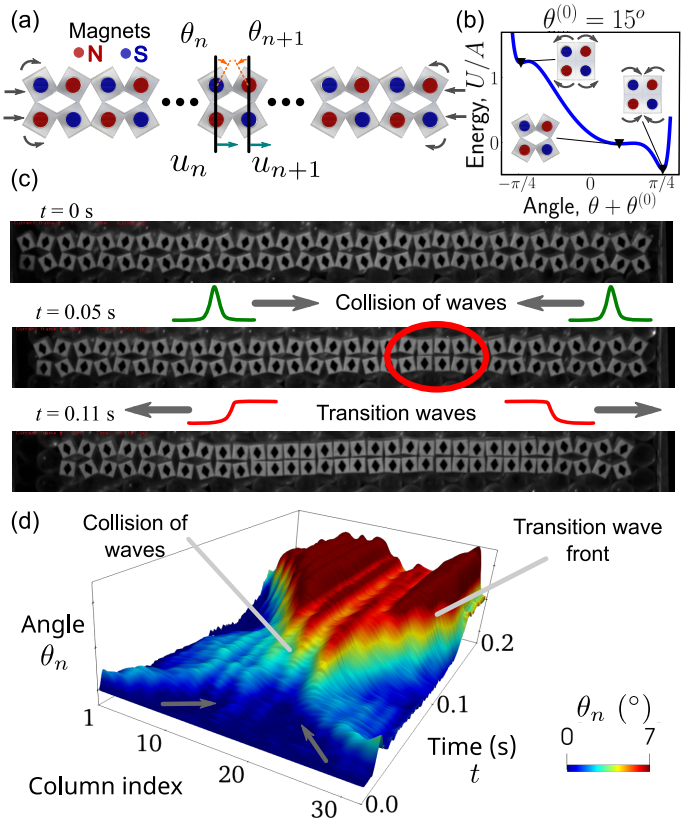

FIG. 1: (a) Schematic illustration of a chain of rotating squares with multistability (in the experiments, this is obtained via embedded magnets). (b) Multistable energy potential for a single complete unit of the chain (comprising two columns of squares that are pre-rotated by $\theta^{(0)} = 15°$) showing three energy minima ($\theta = -60°$, $0°$, and $30°$). (c) Optical images taken with a high-speed camera at times $t = 0$ s, 0.05 s, and 0.11 s. (d) Spatiotemporal plot extracted from the experimental video, showing the rotational angle θ_n for each column n as a function of time.

translational and rotational DOF), which are measured from their (initial) equilibrium state. Here, the initial equilibrium angle is expressed as $\theta^{(0)}$. We 3D print a 32-column chain made of a silicone elastomer using direct ink writing [34]. To achieve multistable behavior, we embed a magnet in each square, resulting in an energy landscape with multiple equilibrium angles (Fig. 1(b)).

To examine the wave interactions, we excite both sides of the chain simultaneously with two impactors. Figure 1(c) shows optical images obtained experimentally via a high-speed camera (Movie 1). We track the angles of each square (θ_n) and plot the results as a function of the column index n and time t, as shown in Fig. 1(d). Initially, the two pulses generated by the impactors propagate inward, toward the center of the chain (see the arrows in Fig. 1(d)). Then, once they meet in the middle of the chain, the collision induces larger rotations of the squares, leading to a phase transformation to another stable state (i.e., the system moves to a different energy minimum in the multistable energy landscape of Fig. 1(b)). Eventually, we observe a phase transformation that grows outward in the form of transition waves. While the propagation of transition waves in mechanical systems has been demonstrated previously, the initiation of these has been restricted to a direct excitation at the boundaries, and never (to our knowledge) via collisions of solitons. Our experimental observation suggests the possibility of controllable nucleation of transition waves at arbitrary locations within the system.

To better understand the experimental observations, we introduce a numerical model and use it to investigate the nonlinear dynamics of colliding waves in this multistable system. First, to describe the interactions between neighboring squares, we model the hinges as a nonlinear spring element composed of axial and torsional springs, expressing the potential function of each hinge element as [17]:

$$U\left(\Delta \boldsymbol{l}, \Delta\theta\right) = \frac{1}{2}k_u|\Delta \boldsymbol{l}|^2 + E_\theta\left(\Delta\theta\right), \tag{1}$$

where $\Delta \boldsymbol{l}$ is the deformation of a linear axial spring with spring constant k_u, and $\Delta\theta = 2\theta$ is the rotational angle of a torsional spring element with energy expressed by the Morse potential function (V_{Morse}) as:

$$E_\theta\left(\Delta\theta\right) = \frac{1}{2}k_\theta(\Delta\theta)^2 + V_{Morse}\left(\Delta\theta\right), \tag{2}$$

$$\begin{aligned} &V_{Morse}\left(\Delta\theta\right) \\ &= A\left\{e^{2\alpha(\Delta\theta - 2\theta_M)} - 2e^{\alpha(\Delta\theta - 2\theta_M)}\right\} \\ &+ A\left\{e^{-2\alpha(\Delta\theta - 2\theta_M)} - 2e^{-\alpha(\Delta\theta_n - 2\theta_M)}\right\}. \end{aligned} \tag{3}$$

Here, k_θ is a linear spring constant. Also A and α are parameters that alter the depth and width of the potential, respectively, and θ_M is a parameter that alters the equilibrium points. Figure 2(a) shows the energy landscape of a single torsional spring element (E_θ) as a function of a hinge rotational angle ($\Delta\theta = 2\theta$) with three energy minima. Here, we denote the energy barrier and its location as E_b and θ_b.

We first consider the propagation of vector solitons in our multistable system by introducing several approximations and taking the continuum limit to derive the nonlinear Klein-Gordon equation. The wave forms of the derived solitary solutions are then compared with those of our numerical simulations. We approximate the potential energy landscape of the rotational spring element by using a 6th-order polynomial (the ϕ^6 model). Then, by employing the traveling coordinate ($X = an - Vt$) and expressing the translational and rotational variables as $B_u(X) = u_n(t)/a$ and $B_\theta(X) = \theta_n(t)$, respectively, we obtain the following nonlinear Klein-Gordon equation for traveling waves:

$$\frac{\partial^2 B_\theta}{\partial X^2} = \eta_1 B_\theta - \eta_3 B_\theta^3 - \eta_5 B_\theta^5 \tag{4}$$

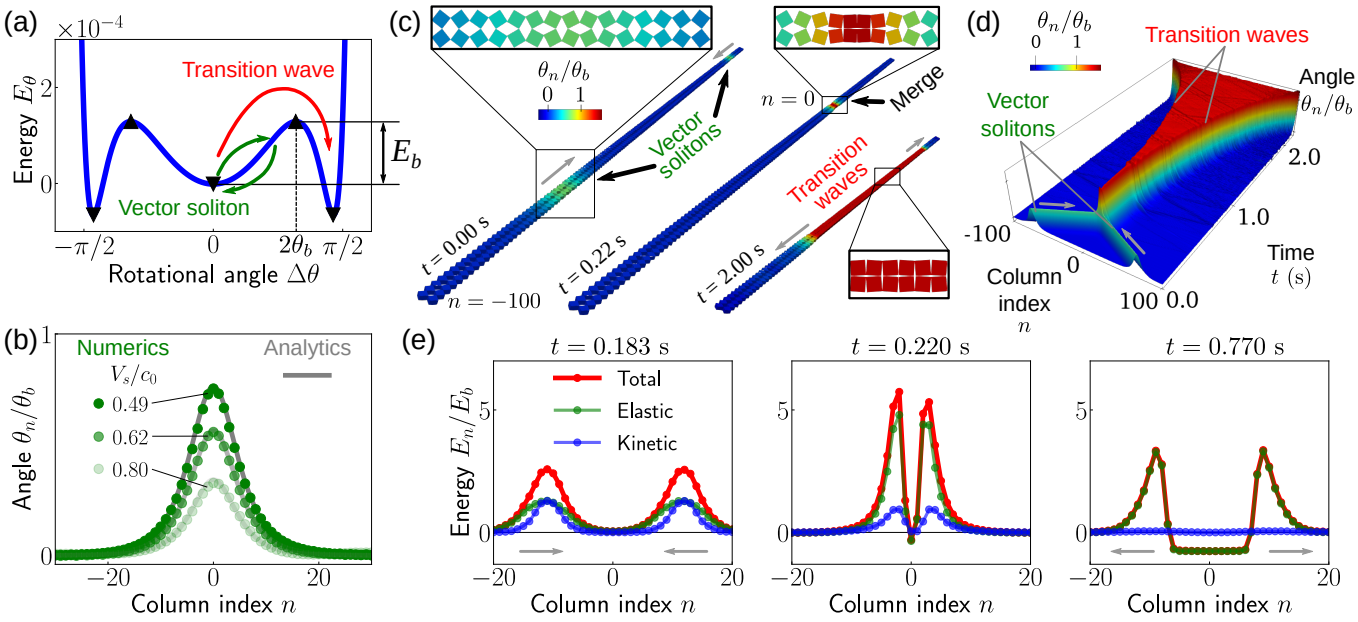

FIG. 2: (a) Multistable energy landscape. E_b indicates the height of the energy barrier that the system needs to overcome to transition from the center energy well to the right one. (b) Angle profiles of solitary waves for three different wave speeds. (c) Snapshots of three-dimensional reconstructions of the numerical simulation at $t = 0.00$, 0.22, and 2.00 s. The insets show the magnified views of a vector soliton propagating in the chain and the center part of the chain after the collision. (d) The spatiotemporal evolution of the propagating waves, shown as the rotational angle of each column of squares as a function of time. (e) Waveforms of colliding waves at i) $t = 0.183$, ii) 0.220, and iii) 0.770 s, plotted as a function of energy and column index.

Note that a relationship between B_u and B_θ (the subscripts u and θ denote translational and rotational motions) holds for traveling waves, i.e., coupling behavior (Note 5 in the Supplemental Material). This nonlinear Klein-Gordon equation supports a soliton solution [35]:

$$B_\theta = \frac{A_\theta \mathrm{sech}(\sqrt{\eta_1}X)}{\sqrt{1 - D\tanh^2(\sqrt{\eta_1}X)}}, \tag{5}$$

where $A_\theta^2 = 2\eta_1(1+D)/\eta_3$ and $(1+D)^2/D = 3\eta_3^2/(4\eta_1\eta_5)$. Note that η_1, η_3, and η_5 are determined by the wave speed and axial/torsional spring constants, which alter both the amplitude A_θ and characteristic width $1/\sqrt{\eta_1}$.

Figure 2(b) shows the rotational angle profiles obtained from the numerical simulation for a chain with 802 columns (green markers) and the soliton solution (solid line) for three different (normalized) wave speeds: $V_s/c_0 = 0.49$, 0.62, and 0.80. The soliton solution based on the potential energy ϕ^6 approximation agrees well with the numerical simulations. Since the rotational DOF is coupled with the translational motion, this solitary wave possesses a vectorial nature.

Next, we study how multiple vector solitons interact with each other. To start, we consider the behavior of vector solitons colliding head-on. We inject two vector solitons with $V_s/c_0 = \pm 0.56$ (i.e., two solitary waves propagating inward) at each end of a chain of 202 columns, and we solve the equations of motion using the fourth-order Runge-Kutta method. Figure 2(c) shows numerically simulated spatiotemporal collision events in the chain (Movie 2). Figure 2(d) plots the extracted rotation of each square, showing two vector solitons initially propagating inward with amplitudes smaller than θ_b (i.e., each remains in the first stable state) and annihilating once they collide at the center of the chain. Several columns show larger rotations than θ_b (i.e., $\theta_n/\theta_b > 1$). The merging solitons thereby form a quasi-static disturbance, nucleating a phase transformation. Immediately after this, transition waves propagate outward from the site of collision, similar to the experimental observations (Fig. 1). Note, the propagation of such transition waves can be altered by tailoring the energy landscape [17].

In addition to the rotational angle profiles, we analyze the collision behavior by considering the energy of each unit. Here, the total energy of the upper-half of the nth square element (T_n) is calculated as $T_n = K_n + E_n$, where K_n is the kinetic energy

$$\begin{aligned} K_n &= \frac{1}{2}M_n\dot{u}_n^2 + \frac{1}{2}J_n\dot{\theta}_n^2, \\ E_n &= U_{n,1}\left(\Delta\boldsymbol{l}_{n,1}, \Delta\theta_{n,1}\right) + \frac{1}{2}U_{n,2}\left(\Delta\boldsymbol{l}_{n,2}, \Delta\theta_{n,2}\right). \end{aligned} \tag{6}$$

Note that for the right-most column, $U_{n,1} = 0$. Figure 2(e) shows the energy profiles consisting of total (T_n), elastic (E_n), and kinetic (K_n) energy components for three different time frames (Movie 3). Before the collision, the vector solitons have kinetic energy equivalent

to their elastic energy. However, during the collision, the kinetic energy of several central units is fully transferred to elastic energy of neighboring units, such that the energy barrier is overcome and the corresponding units jump to another stable state. This triggers the formation of transition waves, in which the elastic energy becomes dominant.

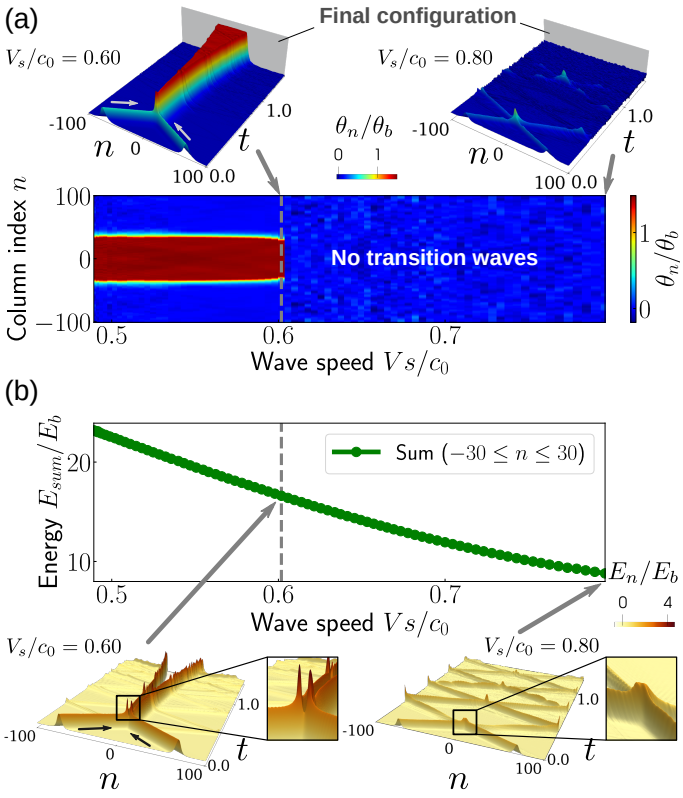

FIG. 3: (a) Collisions of vector solitons with various wave speeds. The surface plot represents the final configurations of the chain at $t = 1.5$ s. The color denotes the normalized angle θ_n/θ_b of each unit cell. (b) Summation of the total energy of a single vector soliton. The insets show the magnified view of the collision.

Next, we analyze the process of transition wave nucleation by varying the amplitude (or equivalently the width or the wave speed) of colliding vector solitons. Note, due to the properties of the vector solitons in this system, specifically their subsonic nature, increasing the soliton velocity is equivalent to decreasing its amplitude, width, and energy. Numerical simulations are performed to examine the final chain configuration at $t = 1.5$ s and to determine whether transition waves are formed or not. Results are plotted as a function of the wave speed V_s/c_0 of the two identical colliding solitons (Fig. 3(a)). Collisions of solitons with wave speeds $V_s/c_0 \lesssim 0.6$ form transition waves, as indicated by the red region in the figure, whereas collisions of faster vector solitons $V_s/c_0 \gtrsim 0.6$ (lower amplitude) do not trigger transition waves. Figure 3(b) shows the total energy carried by a single solitary wave for different wave speeds, which shows an energy threshold corresponding to a total soliton energy of $\sim 16.6E_b$. The existence of this threshold indicates that while most of the kinetic energy is converted into elastic potential energy at the collision location, a minimum number of torsional springs within several units of the collision site need to be "pushed" over the potential barrier separating the stable states in order to induce nucleation.

The inset magnified views of the site of collision in Fig. 3(b) show split energy peaks instead of two waves merging into a single peak, which is a different picture from the superposition of linear waves or even from the classical soliton collision. These features arise from the multistable character of the metamaterial, allowing the colliding solitons to convert into quasi-static transition wave fronts, initially slow and carrying mostly potential elastic energy. Note that wave packets with smaller amplitudes (larger velocity) also emerge from the collision point, as do even smaller amplitude linear waves (Fig. S8).

We also numerically explore other collision scenarios, including head-on and overtaking collisions of vector solitons with distinct wave speeds/amplitudes and rotational directions (or chirality). Similar to Fig. 3(a), we examine the formation of transition waves from two vector solitons propagating from both ends of the chain, with the same chirality but with distinct wave speeds $V_{s1} \neq V_{s2}$ (and, hence, amplitudes). The results are shown in Fig. 4(a), with the red and blue regions indicating that transition waves have or have not nucleated, respectively. Although two colliding solitary waves carry different amounts of energy before the collision, nucleation and propagation of transition waves can be observed (red region). In particular, nucleation takes place easily as we decrease the wave speed of (at least one of) the vector solitons (i.e., larger amplitude).

We also consider different chiralities and propagation directions. For example, vector solitons with opposite rotational directions can propagate simultaneously. The head-on collision of two vector solitons ($V_{s1}/c_0 = 0.49$ and $V_{s2}/c_0 = 0.60$) with the same rotational direction creates transition waves, as we discussed previously (Movie 4). In contrast, if two solitons with opposite rotation collide, the one with larger energy breaks into several components that propagate outward instead of merging or repelling (Fig. 4(b) and Movie 5). Note, if two solitons with opposite rotation propagate at identical (absolute) wave speed, they repel each other (see Fig.S10 in the Supplementary Materials).

Figure 4(c) shows the simulation results for the case in which two vector solitons propagate in the same direction, with the faster soliton ($V_{s2}/c_0 = 0.60$) catching up to the slower soliton. If the rotational directions of the two vector solitons are identical, the overtaking interaction only leads to a shift in phase (Movie 6), similar to classical KdV-type soliton collisions. However, if the vector solitons have opposite rotational directions, the overtaking interaction can lead to the formation of transi-

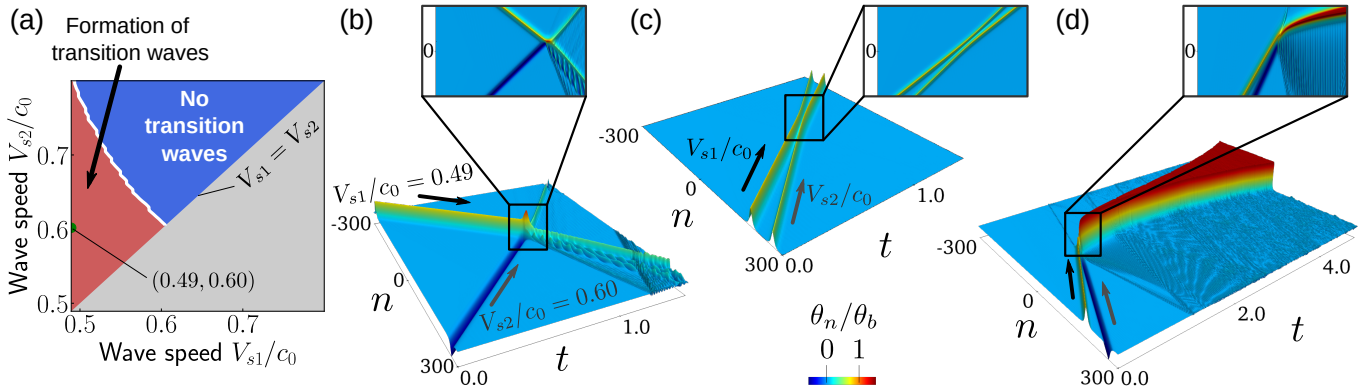

FIG. 4: (a) Collisions of vector solitons with distinct wave speeds ($V_{S1} \neq V_{S2}$, with V_{S1} being the wave speed for the soliton propagating towards $n = 300$ and V_{S2} being the wave speed for the soliton propagating in the opposite direction). Due to symmetry, we investigate only the upper left region. (b) Head-on collision of two vector solitons for the opposite rotation case. We also consider overtaking collisions for (c) same rotation and (d) opposite rotation.

tion waves (Fig. 4(d) and Movie 7), which is the opposite phenomenon than that observed for head-on collisions.

In conclusion, we have studied collisions of elastic vector solitons in a multistable mechanical metamaterial and the process by which these collisions can nucleate phase transitions. Our experimental observations and numerical analyses suggest that there is a threshold of vector soliton amplitude/energy, above which colliding vector solitons will cause nucleation and propagation of transition waves, and below which they will not. Using the validated numerical model, we have also explored different types of nonlinear wave interactions in the multistable system, such as head-on collisions of vector solitons possessing different amplitudes or chiralities (direction of rotation), or collisions of co-propagating solitons. Depending on the specific interaction, the results of these collisions can lead or not lead to conversion to transition waves, demonstrating the richness of this multistable mechanical platform for studying nonlinear waves. Furthermore, we note that this system shows signs of integrability for a range of soliton amplitudes below the energy barrier (KdV soliton-like vector solitons with expected collisional behavior) but also exhibits characteristics of non-integrability when the full tristable multistable potential is explored, as illustrated by the collision of solitons of sufficiently large amplitude, leading to the nucleation of transition waves. Although we have mainly considered the symmetric tristable potential function in this study (in part, because it matches most closely the experimental realization), any asymmetric energy landscapes, including bistable potentials, would also be compatible with collision-induced phase transitions. These additional cases are of interest for exploring more diverse collision scenarios in the future. Such a wide array of effects opens up additional possibilities for fundamental research, by raising questions related to the transposition of these nonlinear processes into higher dimensions, into inhomogeneous or graded metamaterials, or for other nonlinear wave manifestations. Also, our results may be relevant to topological metamaterials (such as twisted structures, graphene [36], etc.), where multistability and the ability to control morphology could allow control of wave propagation (e.g., [37]). One can, in addition, foresee possible future applications of this remote control of transition waves in, e.g., reconfigurable system design in robotics, space structures, medical devices, or in advanced materials for vibration damping, mechanical logic devices, and other emerging areas.

Supplementary Material

Supplemental discussion, figures, and videos available as Supplementary Material online.

Acknowledgements

The authors gratefully acknowledge support via NSF award number 2041410, AFOSR award number FA9550-19-1-0285, and DARPA YFA award number W911NF2010278. H.Y. acknowledges the support of KAKENHI (22K14154). VT acknowledges support from project ExFLEM ANR-21-CE30-0003. H.Y. and H.S. contributed equally to this work.

Data Availability Statement

The data that supports the findings of this study are available within the article and its supplementary material.

Conflict of Interest Statement

The authors have no conflicts to disclose.

[1] E. Fermi, J. Pasta, S. Ulam, and M. Tsingou. Studies of nonlinear problems I. *Technical Report. LA-1940, Los Alamos National Laboratory*, page 20, 1955.

[2] N. J. Zabusky and M. D. Kruskal. Interaction of solitons in a collisionless plasma and the recurrence of initial states. *Phys. Rev. Lett*, 15(6):240–243, 1965.

[3] M. Remoissenet. *Waves Called Solitons: Concepts and Experiments*. Springer, 1996.

[4] C Coste, E Falcon, and S Fauve. Solitary waves in a chain of beads under Hertz contact. *Phys. Rev. E*, 56(5):6104–6117, 1997.

[5] V F Nesterenko. *Dynamics Of Heterogeneous Materials*. Springer-Verlag New York Inc., 2001.

[6] Alessandro Spadoni and Chiara Daraio. Generation and control of sound bullets with a nonlinear acoustic lens. *Proceedings of the National Academy of Sciences*, 107(16):7230–7234, 2010.

[7] E. Avalos and S. Sen. How solitary waves collide in discrete granular alignments. *Phys. Rev. E*, 79(4):046607, 2009.

[8] N. Manton and P. Sutcliffe. *Topological Solitons*. Cambridge University Press, Cambridge, 2004.

[9] Y. Shen and I. Dierking. Recent Progresses on Experimental Investigations of Topological and Dissipative Solitons in Liquid Crystals. *Crystals*, 12(1):94, 2022.

[10] B. Deng, J. R. Raney, K. Bertoldi, and V. Tournat. Nonlinear waves in flexible mechanical metamaterials. *J. Appl. Phys.*, 130(4):040901, 2021.

[11] B. Deng, J. R. Raney, V. Tournat, and K. Bertoldi. Elastic Vector Solitons in Soft Architected Materials. *Phys. Rev. Lett.*, 118(20):204102, 2017.

[12] B. Deng, P. Wang, Q. He, V. Tournat, and K. Bertoldi. Metamaterials with amplitude gaps for elastic solitons. *Nat. Commun.*, 9(1), 2018.

[13] C. Mo, J. Singh, J. R. Raney, and P. K. Purohit. Cnoidal wave propagation in an elastic metamaterial. *Phys. Rev. E*, 100:013001, 2019.

[14] B. Deng, C. Mo, V. Tournat, K. Bertoldi, and J. R. Raney. Focusing and mode separation of elastic vector solitons in a 2D soft mechanical metamaterial. *Phys. Rev. Lett.*, 123(2):24101, 2019.

[15] B. Deng, V. Tournat, P. Wang, and K. Bertoldi. Anomalous collisions of elastic vector solitons in mechanical metamaterials. *Phys. Rev. Lett.*, 122(4):044101, 2019.

[16] J. R. Raney, N. Nadkarni, C. Daraio, D. M. Kochmann, J. A. Lewis, and K. Bertoldi. Stable propagation of mechanical signals in soft media using stored elastic energy. *Proc. Nat. Acad. Sci. USA*, 113(35):9722–9727, 2016.

[17] H. Yasuda, L. M. Korpas, and J. R. Raney. Transition Waves and Formation of Domain Walls in Multistable Mechanical Metamaterials. *Phys. Rev. Appl.*, 13(5):054067, 2020.

[18] L. Jin, R. Khajehtourian, J. Mueller, A. Rafsanjani, V. Tournat, K. Bertoldi, and D. M. Kochmann. Guided transition waves in multistable mechanical metamaterials. *Proc. Nat. Acad. Sci. USA*, 117(5):2319–2325, 2020.

[19] V. Ramakrishnan and M. J. Frazier. Transition waves in multi-stable metamaterials with space-time modulated potentials. *App. Phys. Lett.*, 2020.

[20] O. R. Bilal, A. Foehr, and C. Daraio. Bistable metamaterial for switching and cascading elastic vibrations. *Proc. Nat. Acad. Sci. USA*, 114(18):4603–4606, 2017.

[21] M. J. Frazier and D. M. Kochmann. Atomimetic mechanical structures with nonlinear topological domain evolution kinetics. *Adv. Mater.*, 29:1605800, 2017.

[22] M. Hwang and A. F. Arrieta. Input-Independent Energy Harvesting in Bistable Lattices from Transition Waves. *Sci. Rep.*, 8(1):1–9, 2018.

[23] B. Deng, P. Wang, V. Tournat, and K. Bertoldi. Nonlinear transition waves in free-standing bistable chains. *J. Mech. Phys. Sol.*, page 103661, 2019.

[24] X. Liang, H. Fu, and A. J. Crosby. Phase-transforming metamaterial with magnetic interactions. *Proc. Nat. Acad. Sci. USA*, 119(1):e2118161119, 2022.

[25] A. Zareei, B. Deng, and K. Bertoldi. Harnessing transition waves to realize deployable structures. *Proc. Nat. Acad. Sci. USA*, 117(8):4015–4020, 2020.

[26] J-J Marigo and Lev Truskinovsky. Initiation and propagation of fracture in the models of griffith and barenblatt. *Continuum Mechanics and Thermodynamics*, 16(4):391–409, 2004.

[27] Lev Truskinovsky and Anna Vainchtein. Quasicontinuum models of dynamic phase transitions. *Continuum Mechanics and Thermodynamics*, 18(1):1–21, 2006.

[28] David A Porter and Kenneth E Easterling. *Phase transformations in metals and alloys (revised reprint)*. CRC press, 2009.

[29] RD James. Displacive phase transformations in solids. *Journal of the Mechanics and Physics of Solids*, 34(4):359–394, 1986.

[30] Xiaodan Ren, Jiun-Shyan Chen, Jie Li, TR Slawson, and MJ1236 Roth. Micro-cracks informed damage models for brittle solids. *International journal of solids and structures*, 48(10):1560–1571, 2011.

[31] MF Ashby and CG Sammis. The damage mechanics of brittle solids in compression. *Pure and applied geophysics*, 133(3):489–521, 1990.

[32] N. Nadkarni, A. F. Arrieta, C. Chong, D. M. Kochmann, and C. Daraio. Unidirectional Transition Waves in Bistable Lattices. *Phys. Rev. Lett.*, 116(24):244501, jun 2016.

[33] L. M. Korpas, R. Yin, H. Yasuda, and J. R. Raney. Temperature-Responsive Multistable Metamaterials. *ACS Applied Materials and Interfaces*, 13(26):31163–31170, 2021.

[34] S. Shan, S. H. Kang, J. R. Raney, P. Wang, L. Fang, F. Candido, J. A. Lewis, and K. Bertoldi. Multistable Architected Materials for Trapping Elastic Strain Energy. *Adv. Mater.*, 27(29):4296–4301, 2015.

[35] A. Khare and A. Saxena. Domain wall and periodic solutions of a coupled ϕ^6 model. *J. Math. Phys.*, 49:063301, 2008.

[36] Shuyang Dai, Yang Xiang, and David J Srolovitz. Twisted bilayer graphene: Moiré with a twist. *Nano letters*, 16(9):5923–5927, 2016.

[37] A. A. Watkins, A. Eichelberg, and O. R. Bilal. Harnessing Reprogrammable Phase Transitions to Control the Propagation of Sound Waves. *Phys. Rev. Appl.*, 17:024036, 2022.